Finite-time magnetometer bias estimation using angular rates measurements

Giuseppe Fedele, IEEE member, Luigi D'Alfonso, Gaetano D'Aquila, IEEE member

***Abstract*—This paper deals with the problem of estimating the hard iron bias affecting the measurements provided by a tri-axial magnetometer. The output of this kind of sensors is always affected by anomalies caused by fabrication issues (e.g. sensor axes misalignment and different sensitivity on each sensor axis) and by external perturbations on the magnetic field. As a consequence, magnetometer measurements are corrupted by a measurement bias, denoted as hard iron distortion, due to magnetic deviations induced by the host platform and by objects that produce a constant magnetic field, like permanent magnet, speakers or pieces of magnetized material which can be found in the sensor environment. These anomalies motivate for a sensor calibration procedure which has to be performed before its use in real applications. However, while in principle this calibration should be carried out only for one time, in a realistic point of view, the sensor environment may be subject to change over time, for example due to ambient temperature variation, which, along with long-term drifts, may cause a further distortion on magnetometers data with a resulting variation in the hard iron bias. Therefore the calibration procedure has to be periodically repeated. In this context, this paper proposes two procedures able to estimate the hard iron bias in finite-time. In particular this kind of algorithms may be used after a standard calibration, to estimate the varied hard iron bias. Standard calibration procedures require special sensor movements to be performed. On the contrary, both the solutions, described in this paper, can be used during standard sensor use, with no specific required movements to be ensured. The two proposed algorithms ensure finite-time estimation performance and robustness against measurements noise. The effectiveness of the described solutions is proved by numerical simulations and experimental tests carried out using a real magnetometer sensor.**

I. Introduction

Magnetometers are commonly used to measure Earth's local magnetic field vector so that to obtain the orientation of a body w.r.t. the magnetic North. One of the first magnetic compasses was proposed in China thousands of years ago; it was made of a bowl filled with water, used as a leveling platform, and a magnetic lodestone placed on a plate floating on the water [1].

Thanks to their low power, light weight and potential for low cost manufacture, Micro-Electro-Mechanical Systems components are widely used nowadays and they open up a wide range of applications of the inertial measurements units (IMUs). Magnetometers are a key aiding sensor for attitude estimation in low-cost, high performance navigation systems [2], with widespread application to autonomous air, ground and ocean vehicles. These inexpensive, low power sensors allow for accurate attitude aiding by comparing the magnetic field vector observation in body coordinates with the vector representation in Earth coordinates [3]. Almost every spacecraft has been flown with a magnetometer whose application is scientific and/or for implementing attitude maneuvers. Sometimes the satellite carries two of them, which may be used for gradient measurements of magnetic natural signatures, for compensation of satellite-body disturbances or for in-flight calibration.

In particular, there is a considerable body of work on using tri-axial field sensors (magnetometers and accelerometers) in robotics [4], and control applications [5], virtual reality, gaming systems. In the literature, significant works can be found on attitude heading reference systems for aerospace applications [6] too. An excellent review of attitude filters is given by Crassidis et al. [7].

However, a very common problem with magnetometers is related to measurements distortions due to external perturbations on the magnetic field [8]. As a consequence, the measurements provided by IMU systems, are affected by magnetic distortions and non ideal sensor effects like non-orthogonality and general time-varying bias. In a realistic point of view, each magnetometer is affected by distortions related to sensor fabrication issues like axes misalignment and different sensitivity on each sensor axis, this anomaly is used denoted as soft iron. Moreover the obtained magnetic field measurements are also corrupted by a measurement bias, denoted as hard iron perturbation, due to distortions related to sensor fabrication issues and the magnetic deviations induced by the host platform [9], [10]. These distortions are created by objects that produce a constant magnetic field. For instance permanent magnet, speakers or pieces of magnetized material will cause a hard iron distortion. If the magnetized material is physically attached to the same reference frame as the sensor, then this type of hard iron distortion will cause a constant offset in the sensor output. Hard iron bias magnitude can easily be 10 times or greater compared to earths magnetic field. These issues hinder the sensor usability and motivate several calibration techniques to be performed before they are used.

Calibration problem is usually faced by means of two kinds of techniques. The first one, which has been firstly developed, requires precise external reference and may be costly (the main example in this context is the swinging method [9]). To reduce the cost of the calibration procedures, many studies focus on methods requiring no external equipment or references. This second kind of calibration techniques is referred as self-calibration or auto-calibration [11], [12], [13] and reached interest in recent years. Without a precision reference, the input of the sensor is unknown, thus the self-calibration methods usually make use of a time-invariant vector field,

G. Fedele is with the Department of Informatics, Modeling, Electronics and Systems Engineering, University of Calabria, Italy E-mail: *giuseppe.fedele@unical.it*

L. D'Alfonso, G. D'Aquila are with GiPStech s.r.l, Italy, E-mail: {*l.dalfonso,g.daquila*}*@gipstech.com*

e.g. the Earth's magnetic field for the magnetometers. Since the magnetometer should measure a constant local magnetic field vector, when rotating a magnetometer, its measurements should lie on a sphere. However, the presence of magnetic disturbances or magnetometer sensor errors leads to an ellipsoid of data instead. The problem is now solved by optimality criteria and the constant strength of the vector field is used as a constraint in the calibration.

The calibrating procedure consists of rotating the sensor around three axes in the space keeping its center of gravity fixed and acquiring measurements so that to obtain the coefficients of the magnetometer [14]. Obviously to achieve accurate calibration the constellation of data points has to spread enough over the full $3D$ space so that to effectively fit the ellipsoid. As a consequence, the calibration procedure may be very tedious and it may require time to be correctly performed. These methods are also known as ellipsoid fitting methods [15], [16], [17], [18]. In particular, the problem of fitting an ellipsoid of data to a sphere was considered for example by [19] where the authors show that the ordinary least squares estimate is inconsistent when using measurements corrupted by noise. Then different calibration approaches have been developed to overcome this problem, see e.g. [9], [20]. Earlier mathematical methods using the scalar field as a reference had been developed, but these have nonlinear iterative solutions, which may lead to problems with convergence, uniqueness and stability (see [21]).

In [22], [23], the magnetometer reading error model is discussed and formulated to account for the combined effect of modeled and unmodeled linear time-invariant magnetic transformations. The calibration problem is faced by estimating the parameters of an ellipsoid manifold using a Maximum Likelihood Estimator starting from the sensor readings.

Recent calibration techniques have solved the calibration problem using two main steps. For example in [24], a TWOSTEP batch method is proposed which is based on the observations of the differences between the norms of the modeled and the measured vectors, denoted as scalar-checking. In the first step of the algorithm, the centering approximation suggested by [25] produces a good initial guess of the calibration parameters, by rewriting the calibration problem in a linear least squares form. In a second step, a batch Gauss-Newton method is adopted to iteratively estimate the bias, scaling and non-orthogonality parameters.

After the calibration procedure has been performed, an estimation of the scaling factors, of the sensors' axes misalignment and of the sensors' sensitivities on each axis is obtained and can be used while sensor is taking measurements. However, as explained in [26], the sensor environment may be subject to change over time, for example due to ambient temperature variation, which, along with long-term drifts or any other possible change dependent on other physical quantities, may cause a further distortion on magnetometers data. Indeed magnetometer measurements are prone to drift over temperature and although the temperature coefficients of these devices are minimized by design, these parameters should be taken into account. These anomalies are modeled by including an offset on the hard iron perturbation[27]. These variations on the magnetometer bias are usually very slow over time but if not taken into account they can have a drastic effect on the sensor measurements. In order to decrease the impact of environment variations on the hard iron bias estimate, the traditional calibration procedures require a data constellation of recent magnetic measurements and the calibration is required to be periodically repeated, with a resulting time cost due to the requirements of collecting many data points all over the $3D$ space.

In this context, a procedure able to estimate a further offset on the bias could be helpful. In particular this kind of algorithm may be used after a standard calibration, to adapt the hard iron bias estimation to the described variations.

Aim of this paper is to propose novel solutions to dynamically adapt the hard iron bias to environment variations. More precisely, the proposed algorithms will avoid to repeat the sensor calibration procedure. The new bias estimation techniques will:

- not require any assumptions on the movements/rotations performed by the sensor during the estimation procedure;
- not assume any knowledge on the real magnetic field value;
- not require knowledge about the attitude of the sensor;
- ensure finite-time estimation in providing an exact estimation of the hard iron bias.

To this end, two approaches will be proposed using both measurements by a magnetometer and a gyroscope on the same inertial measurement unit. The first one uses modulating functions to provide a batch bias estimation. In particular the results presented in [28], [29] are adapted to the magnetometer bias estimation. The second approach exploits Volterra Integral Operators and the results obtained in [30], [31] with a resulting estimation algorithm able to give exact deadbeat estimation of the hard iron bias.

The paper is organized as follows: in Section II the problem is stated; in Section III a batch solution to the estimation problem is proposed; in Section IV a real time bias estimation algorithm is described; in Section V numerical and experimental results are shown and in Section VI conclusions are drawn.

II. Problem statement

Let $\tilde{m}(t)$ be the real earth field which should be measured by the magnetometer, the obtained measurement by the sensor can be modeled as

$$m^*(t) = A(\tilde{m}(t) + b) \tag{1}$$

where $b \in \mathbb{R}^3$ is a constant vector representing the ferromagnetic bias affecting the sensor measurement and $A \in \mathbb{R}^{3\times 3}$ is a matrix representing the axes misalignment, the measurement scaling w.r.t. the magnetic field module and the sensitivities on each sensor axis.

The problem of magnetometer calibration consists in defining a procedure able to obtain an estimation $\hat{A}, \hat{b}$ as more coherent as possible with the real couple A, b so that by computing

$$\hat{m}(t) = \hat{A}^{-1} m^*(t) - \hat{b} \tag{2}$$

the obtained measurement is $\hat{m}(t) \approx \tilde{m}(t)$.

Let now m_0 be the reference magnetic vector in the North-East-Down (NED) reference frame[1] reference frame (note that this vector is locally constant on the earth' plane). Given the transformation matrix $R(t)$ representing the rotations, at time t, from the sensor reference frame to the NED reference frame, by rotating the measurements from the sensor to NED reference frame and using (1) it follows that

$$m_0 = R(t)(A^{-1}m^*(t) - b).$$

Since the matrix A is assumed to be known thanks to a starting calibration performed in a traditional way, in the following, for the sake of notation simplicity, let

$$m(t) = A^{-1}m^*(t)$$

yielding to

$$m_0 = R(t)(m(t) - b). \tag{3}$$

Starting from the above model, by deriving both sides w.r.t. time it follows that

$$0 = \dot{R}(t)(m(t) - b) + R(t)\dot{m}(t). \tag{4}$$

Using properties (A.39) and (A.36):

$$S_\omega(t)b = S_\omega(t)m(t) + \dot{m}(t) \tag{5}$$

where $S_\omega(t) = S(\omega(t))$ and $\omega(t) = [\omega_x(t), \omega_y(t), \omega_z(t)]$ is the vector of angular rotations rates about the three axes provided by a gyroscope.

Starting from the above equation, aim of this work is to obtain an estimation of b by using auxiliary signals in the place of the unmeasurable time-derivative of $m(t)$.

III. Batch solution for bias estimation

Let T_w be the observation time of the acquired measurements. This time is divided into N sub intervals of $T = \frac{T_w}{N}$ seconds. For each time interval $q = 1, \ldots, N$, defined by $t \in [(q-1)T, qT)$, by applying the inner product defined in (A.41) to the equation (5) it holds that

$$\begin{aligned}\left[\int_0^T \phi_K(\tau)S_\omega(\tau + (q-1)T)d\tau\right] b = \\ = \int_0^T \phi_K(\tau)(S_\omega(\tau + (q-1)T)m(\tau + (q-1)T) + \\ + \dot{m}(\tau + (q-1)T))d\tau.\end{aligned} \tag{6}$$

Using equation (A.42), it follows that

$$\begin{aligned}\left[\int_0^T \phi_K(\tau)S_\omega(\tau + (q-1)T)d\tau\right] b = \\ = \int_0^T \phi_K(\tau)S_\omega(\tau + (q-1)T)m(\tau + (q-1)T)d\tau + \\ - \int_0^T \dot{\phi}_K(\tau)m(\tau + (q-1)T)d\tau.\end{aligned} \tag{7}$$

[1]A reference frame where the x-axis points to the geographical north, the z-axis points downward to the earth center and the y-axis is computed to comply with the right-hand rule

which can be rewritten as

$$G_q b = \zeta_q \tag{8}$$

where

$$\begin{aligned}G_q &= \left[\int_0^T \phi_K(\tau)S_\omega(\tau + (q-1)T_w)d\tau\right], \\ \zeta_q &= \int_0^T \phi_K(\tau)S_\omega(\tau + (q-1)T_w)m(t)d\tau + \\ &\quad - \int_0^T \dot{\phi}_K(\tau)m(\tau + (q-1)T_w)d\tau.\end{aligned}$$

The following matrices can be now defined

$$\mathcal{G} = \begin{bmatrix} G_1 \\ \vdots \\ G_N \end{bmatrix}, \ \mathcal{Z} = \begin{bmatrix} \zeta_1 \\ \vdots \\ \zeta_N \end{bmatrix}$$

yielding to

$$\mathcal{G}b = \mathcal{Z}. \tag{9}$$

The solution

$$\hat{b} = \mathcal{G}^\dagger \mathcal{Z}. \tag{10}$$

represents a least mean square approximation of the hard iron bias.

IV. Real time solution for Bias estimation

Let now apply the Volterra operator to both sides of equation (5) so that to obtain

$$[V_K S_\omega b](t) = [V_K S_\omega m](t) + [V_K \dot{m}](t).$$

Since in the above equation a first derivative term is involved, using the Kernel

$$K(t, \tau) = e^{-\rho(t-\tau)}(1 - e^{\rho\tau})$$

it follows that

$$[V_K S_\omega](t)b = [V_K S_\omega m](t) + K(t,t)m(t) - [V_{K^{(1)}} m](t). \tag{11}$$

Moreover the terms of equation (11) can be easily obtained by applying equation (A.46); the terms $[V_K S_\omega](t)$ and $[V_K S_\omega m](t)$ can be seen as

$$\begin{aligned}[V_K S_\omega](t) &= \frac{1}{s+\rho}[K(t,t)S_\omega(t)], \\ [V_K S_\omega m](t) &= \frac{1}{s+\rho}[K(t,t)S_\omega(t)m(t)]\end{aligned} \tag{12}$$

where the s is the Laplace variable and the notation $P(s)[u(\cdot)]$ stands for the time-domain output of the system $P(s)$ with input $u(\cdot)$. Using equation (A.54) the term $[V_{K^{(1)}} m](t)$ can be obtained as

$$[V_{K^{(1)}} m](t) = \frac{1}{s+\rho}[K^{(1)}(t,t)m(t)]. \tag{13}$$

Note that the signal

$$\alpha(t) = K(t,t)m(t) - [V_{K^{(1)}} m](t) + [V_K S_\omega m](t)$$

can be computed in real time and it can be assumed to be known since it is not related with the constant bias b.

Defining the matrix $H(t) = [V_K S_\omega](t) \in \mathbb{R}^{3\times 3}$, the equation (11) can be rewritten as

$$H(t)b = \alpha(t). \tag{14}$$

Assumption 1 *(Persistency of Excitation): The matrix $H(t)$ is persistently exciting (PE) in $\mathbb{R}^{3\times 3}$ in the sense that exsists constans $r > 0$ and $T > 0$ such that $\forall t \geq 0$*

$$\int_{t-T}^{t} H^T(\tau)H(\tau)d\tau \geq rI > 0. \tag{15}$$

Note that $H(t)$ is by definition a skew-symmetric matrix $\in \mathbb{R}^{3\times 3}$ and, by the Jacobi's theorem [**?**], it does not have full rank. However, under the Assumption 1, a filtered version of the matrix $H^T(t)H(t)$ characterizes a sufficiently informative output signal at time t since it is a definite positive matrix; as a consequence, the matrix $H^T(t)H(t)$ has full rank.

To benefit of the persistent excitability of $H(t)$, the equation (14) is modified by multiplying both sides by $H^T(t)$, yielding to

$$H^T(t)H(t)b = H^T(t)\alpha(t). \tag{16}$$

Let $\beta(t) = H^T(t)\alpha(t)$ and $M(t) = H^T(t)H(t)$ so that the above equation becomes

$$M(t)b = \beta(t) \tag{17}$$

which implies that the following constraint has to be verified

$$M(t)b - \beta(t) = 0. \tag{18}$$

Two filtered version, $M_f(t)$ and $\beta_f(t)$, of the matrices $M(t)$ and $\beta(t)$ respectively, are now defined as

$$\begin{cases} \dot{M}_f(t) &= -\lambda M_f(t) + M(t) \\ \dot{\beta}_f(t) &= -\lambda \beta_f(t) + \beta(t) \end{cases} \tag{19}$$

with $\lambda \in \mathbb{R}_{>0}$, $M_f(0) = 0 \in \mathbb{R}^{3\times 3}$ and $\beta_f(0) = 0 \in \mathbb{R}^3$. Starting from equation (18) and substituting the signals $M(t)$ and $\beta(t)$ with their filtered versions, the resulting constraint

$$M_f(t)b - \beta_f(t) = 0 \tag{20}$$

is satisfied too.

Given an estimate $\hat{b}(t)$, $\hat{b}(t) \neq b$ in general, the constraint (20) is not verified due to a residual

$$E(t) = M_f(t)\hat{b}(t) - \beta_f(t), \tag{21}$$

with

$$\dot{E}(t) = \dot{M}_f(t)\hat{b}(t) + M_f(t)\dot{\hat{b}}(t) - \dot{\beta}_f(t). \tag{22}$$

To make $|E(t)| \to 0$ in finite-time the following sliding-mode type adaptation law can be used:

$$\dot{\hat{b}}(t) = M_f^{-1}(t)(-\mu\ sign(E(t))\sqrt{|E(t)|} + \dot{\beta}_f(t) - \dot{M}_f(t)\hat{b}(t)) \tag{23}$$

when $det(M_f(t)) > \varepsilon$ and $\varepsilon > 0$ is a user-defined threshold constant.

Note that under the Assumption 1, the matrix $M_f(t)$ has full rank and, as a consequence, computing the matrix $M_f^{-1}(t)$ is allowed.

A. finite-time convergence in noise-free scenario

In this section, the convergence properties of the proposed bias estimator in absence of external perturbations is addressed.

Lemma 1 *Given a vector $x = [x_1, \ldots, x_n] \in \mathbb{R}^n$ and $p \in (0, 1)$, it holds that*

$$\sum_{i=1}^{n} |x_i|^p \geq \left(\sum_{i=1}^{n} |x_i|\right)^p. \tag{24}$$

Theorem 1 *If Assumption 1 holds, given the noise-free signals $m(t), \omega(t)$, the estimated bias $\hat{b}(t)$ governed by the adaptation law* (23) *converges to the true value b in finite-time.*

Proof: Let define the following Lyapunow function

$$V(t) = \frac{1}{2}E^T(t)E(t), \tag{25}$$

the derivative of which is

$$\dot{V}(t) = E(t)\dot{E}(t). \tag{26}$$

Using (22) and substituting (23) in (25) it follows that

$$\dot{V}(t) = -\mu||E(t)||_{\frac{3}{2}}^{\frac{2}{3}} = -\mu\sum_{i=1}^{3}|E_i(t)|^{\frac{3}{2}} \tag{27}$$

where $E_i(t)$ is the i-th component of $E(t)$.

$\dot{V}(t)$ can now be written in terms of $V(t)$. Starting from (27), one obtains that

$$\begin{aligned} \dot{V}(t) &= -\mu\sum_{i=1}^{3}|E_i(t)|^{\frac{3}{2}} = -\mu\sum_{i=1}^{3}(|E_i(t)|^2)^{\frac{3}{4}} = \\ &= -2^{\frac{3}{2}}\mu\sum_{i=1}^{3}\left(\frac{1}{2}|E_i(t)|^2\right)^{\frac{3}{4}}. \end{aligned} \tag{28}$$

Applying Lemma 1, the equation (28) becomes

$$\dot{V}(t) = -2^{\frac{3}{2}}\mu\sum_{i=1}^{3}\left(\frac{1}{2}|E_i(t)|^2\right)^{\frac{3}{4}} < -2^{\frac{3}{2}}\mu\left(\sum_{i=1}^{3}\left(\frac{1}{2}|E_i(t)|^2\right)\right)^{\frac{3}{4}}. \tag{29}$$

Using now (25)

$$\begin{aligned} \dot{V}(t) &< -2^{\frac{3}{2}}\mu\left(\sum_{i=1}^{3}\left(\frac{1}{2}E_i(t)^2\right)\right)^{\frac{3}{4}} = -2^{\frac{3}{2}}\mu\left(\frac{1}{2}||E(t)||_2^2\right)^{\frac{3}{4}} \\ &= -2^{\frac{3}{2}}\mu(V(t))^{\frac{3}{4}} \end{aligned} \tag{30}$$

and thus the proof follows. The convergence time can be easily obtained as shown in Lemma 3. ■

B. Robustness Analysis

In this section, the stability properties of the proposed estimation technique, in the case of noisy measurements, are studied.

Aiming at characterizing the proposed algorithm robustness in facing measurement perturbations, the stability analysis will be performed under the assumption that both $m(t)$ and $\omega(t)$ are affected by bounded additive disturbances:

$$\begin{aligned}\overline{m}(t) &= m(t) + d_m(t)\\ \overline{\omega}(t) &= \omega(t) + d_\omega(t)\end{aligned}$$

where $|d_m(t)| \leq \overline{d}_m$ and $|d_\omega(t)| \leq \overline{d}_\omega$.

Starting from equations (12) and (13) and introducing the perturbation, it follows that

$$\begin{aligned}[V_K S_\omega](t) &= \frac{1}{s+\rho}[K(t,t)(S_\omega(t) + \Delta S_\omega(t))] =\\ &= \frac{1}{s+\rho}[K(t,t)S_\omega(t)] + \frac{1}{s+\rho}[K(t,t)\Delta S_\omega(t)],\end{aligned} \tag{31}$$

$$\begin{aligned}[V_K S_\omega m](t) =& \frac{1}{s+\rho}[K(t,t)(S_\omega(t) + \Delta S_\omega(t))(m(t) + d_m(t))] =\\ &= \frac{1}{s+\rho}[K(t,t)S_\omega(t)m(t)] +\\ &+ \frac{1}{s+\rho}[K(t,t)(S_\omega(t)d_m(t) + \Delta S_\omega(t)\overline{m}(t))],\end{aligned} \tag{32}$$

$$\begin{aligned}[V_{K^{(1)}} m](t) &= \frac{1}{s+\rho}[K^{(1)}(t,t)(m(t) + d_m(t))] =\\ &= \frac{1}{s+\rho}[K^{(1)}(t,t)m(t)] + \frac{1}{s+\rho}[K^{(1)}(t,t)d_m(t)]\end{aligned} \tag{33}$$

where $\Delta S_\omega(t) = S(d_\omega(t))$ is computed using equation (A.38) and the noise $d_\omega(t)$; since $d_\omega(t)$ is bounded, $\Delta S_\omega(t)$ is bounded too.

As shown by the previous equations, the perturbation on the measurements can be seen as a noisy input to the dynamic system $\frac{1}{s+\rho}$. Thanks to the linearity and to the internal stability of this system, the output due to this noisy bounded input will be bounded too. As a consequence the signals $\alpha(t)$ and $H(t)$ become

$$\begin{aligned}\overline{\alpha}(t) &= \alpha(t) + \Delta\alpha(t)\\ \overline{H}(t) &= H(t) + \Delta H(t)\end{aligned}$$

where

$$\begin{aligned}\Delta\alpha(t) &= K(t,t)d_m(t) + \frac{1}{s+\rho}[K(t,t)(S_\omega(t)d_m(t) +\\ &+ \Delta S_\omega(t)\overline{m}(t)) - K^{(1)}(t,t)d_m(t)]\end{aligned}$$

and

$$\Delta H(t) = \frac{1}{s+\rho}[K(t,t)\Delta S_\omega(t)]$$

are related to the measurements noises and are bounded too since they are computed as the sum of bounded signals.

Let now assume that $\overline{H}(t)$ is persistently exciting in $\mathbb{R}^{3\times3}$; at this point the signals

$$\begin{aligned}\overline{\beta}(t) &= \overline{H}^T\overline{\alpha}(t) = \beta(t) + \Delta\beta(t)\\ \overline{M}(t) &= \overline{H}^T(t)\overline{H}(t) = M(t) + \Delta M(t)\end{aligned}$$

can be used instead of their nominal versions to define

$$\begin{cases}\dot{\overline{M}}_f(t) &= -\lambda\overline{M}_f(t) + \overline{M}(t)\\ \dot{\overline{\beta}}_f(t) &= -\lambda\overline{\beta}_f(t) + \overline{\beta}(t)\end{cases}$$

and the following sliding-mode type adaptation law

$$\dot{\hat{b}}(t) = \overline{M}_f^{-1}(t)(-\mu\ sign(\overline{E}(t))\sqrt{|\overline{E}(t)|} + \dot{\overline{\beta}}_f(t) - \dot{\overline{M}}_f(t)\hat{b}(t)) \tag{34}$$

which ensures that the residual

$$|\overline{E}(t)| = |\overline{M}_f(t)\hat{b}(t) - \overline{\beta}_f(t)| \to 0$$

in finite-time.

As a consequence, the estimation $\hat{b}(t)$ converges in finite-time in the bounded region

$$\hat{b}(t) \in \left[\inf_{0\leq\tau\leq t}(\overline{M}_f(\tau))^{-1}\overline{\beta}_f(\tau),\ \sup_{0\leq\tau\leq t}(\overline{M}_f(\tau))^{-1}\overline{\beta}_f(\tau)\right]. \tag{35}$$

In conclusion, the estimation error $\hat{b}(t) - b$ is bounded with respect to bounded disturbances.

V. Numerical and experimental results

To test the proposed hard iron bias estimation algorithms, numerical simulation in a simulated environment and experimental tests using real inertial sensors have been performed.

The batch bias estimation algorithm proposed in Section III, has been used in a sliding mode technique translating the measurements data of T seconds and running the algorithm on the resulting translated observation window.

A. Numerical results

In the numerical tests, inertial data have been generated using Matlab/Simulink *6DOF(Quaternion)* in the Aerospace Blockset^{TM} [32]. The sensor body has been assumed to be forced with three moments and three forces, a moment and a force for each axis.

The simulated moments are

$$\begin{aligned}M_x(t) &= 0.5\ square(\tfrac{\pi}{10}t, 50)\ Nm,\\ M_y(t) &= 0.2\ sawtooth(t, 0.5)\ Nm,\\ M_z(t) &= 0.2\ chirp(t, 1, \tfrac{T_{sim}}{2}, 3)\ Nm\end{aligned}$$

on the x, y, z axis respectively. The function $square(t,\delta)$ is a square wave with specified duty cycle, δ; $sawtooth(t,\nu)$ is a modified triangle wave where ν determines the point between 0 and 2π at which the maximum occurs; $chirp(t, f_0, t_1, f_1)$ generates samples of a linear swept-frequency cosine signal at the time instances defined in array t, where f_0 is the instantaneous frequency at time 0, and f_1 is the instantaneous

frequency at time t_1, T_{sim} is the simulation time which has been set to $100s$. The simulated forces are

$$F_x(t) = 10\ N; \quad F_y(t) = 0\ N; \quad F_z(t) = 0\ N$$

on the three sensor axes. Note that the proposed moments and forces do not keep the sensor center of gravity fixed; as a consequence, the measurements acquired during the movements due to these moments/forces could not be used in a traditional sensor calibration algorithm.

Sensor measurements are affected by the hard iron bias

$$b(t) = \begin{cases} b_1 = [\ 940, \quad 235, \quad 564\ ]^T\ \mu T & \text{if } t \leq \frac{T_{sim}}{2} \\ b_2 = [\ -470, \quad 47, \quad -47\ ]^T\ \mu T & \text{if } t > \frac{T_{sim}}{2} \end{cases}$$

The variation at $t = \frac{T_{sim}}{2}$ simulates a sensor environment change with a resulting new hard iron bias.

The parameters for the real-time deadbeat bias estimation algorithm proposed in Section IV have been set to

$$\mu = 0.5, \quad \lambda = 0.5, \quad \rho = 1, \quad \varepsilon = 10^{-5};$$

for the sliding estimation algorithm, based on the solution proposed in Section III, the parameters have been set to

$$K = 6, \quad T_w = 10s, \quad T = 1s.$$

Figs. 1, 2, 3 show the estimation results on x-axis, y-axis, z-axis respectively using the proposed solutions.

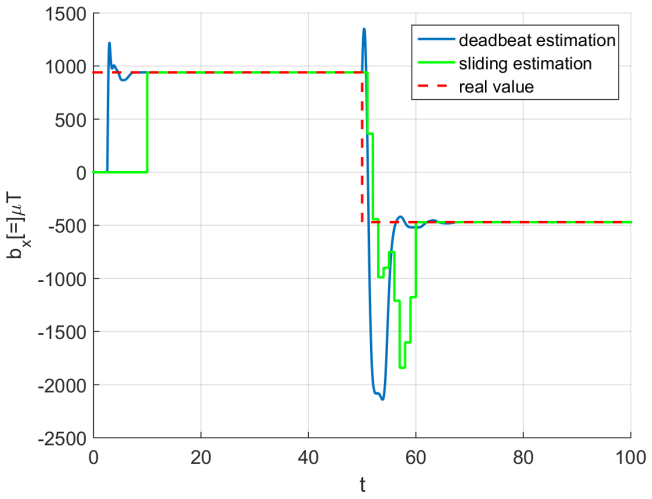

Fig. 1. Estimation results on x-axis in noise-free scenario

Results show that both the described algorithms provide an estimation $\hat{b}(t)$ which adapts itself to the hard iron bias variation occurred in $t = \frac{T_{sim}}{2}$.

As a second test, the same environment has been simulated adding the bounded uniformly distributed noises

$$d_m(t) \leq 10\mu T, \quad d_\omega \leq 1 rad/s$$

to the measurements provided by the magnetometer and the gyroscope respectively. Figs. 4, 5, 6 show the estimation results in this noisy scenario. For the sake of clarity, in Fig. 7 the

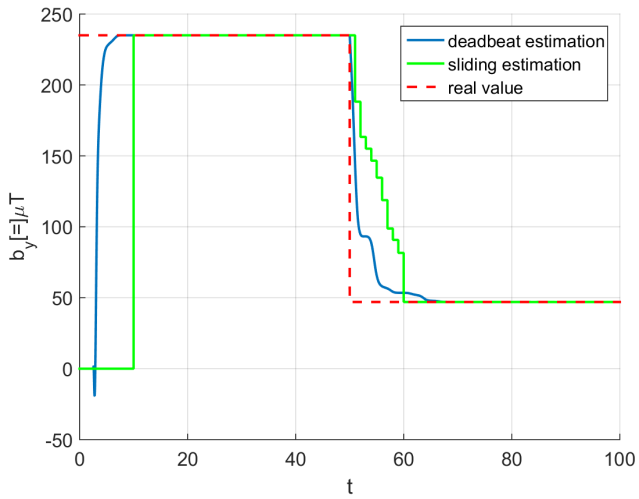

Fig. 2. Estimation results on y-axis in noise-free scenario

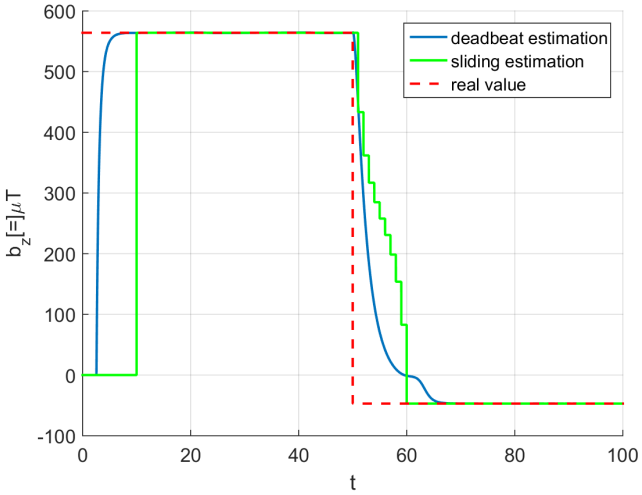

Fig. 3. Estimation results on z-axis in noise-free scenario

estimation is depicted by showing a magnification of the results on a given time interval.

Once again, the estimation is effective in both the deadbeat and the sliding cases.

B. *Experimental results*

To furtherly test the proposed estimation techniques, a real experiment acquiring measurements with the inertial measurement unit equipped on the smarthphone Google Nexus 5, has been performed.

In particular, first of all a calibration has been carried out in the traditional way using the algorithm proposed in [33] so that to obtain an estimation $\tilde{A}, \tilde{b}$ of the matrix A and of the bias b. As a second step, using the matrix $\tilde{A}$, the proposed solutions to the hard iron bias estimation problem have been used to provide an estimate $\hat{b}(t)$ of the bias. The measurements used by the proposed algorithms have been acquired during a standard walk, while the user was making a phone-call, then

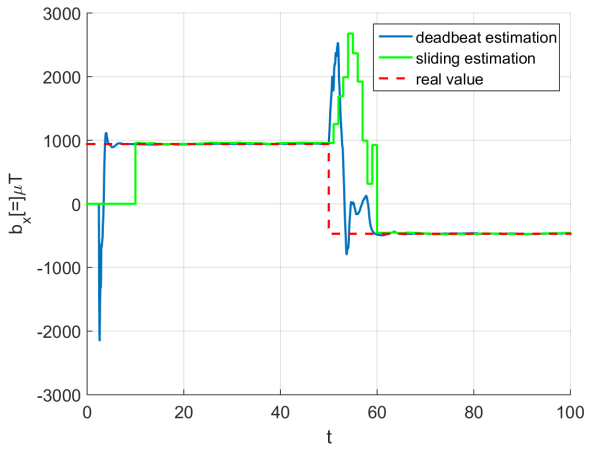

Fig. 4. Estimation results on x-axis in noisy scenario

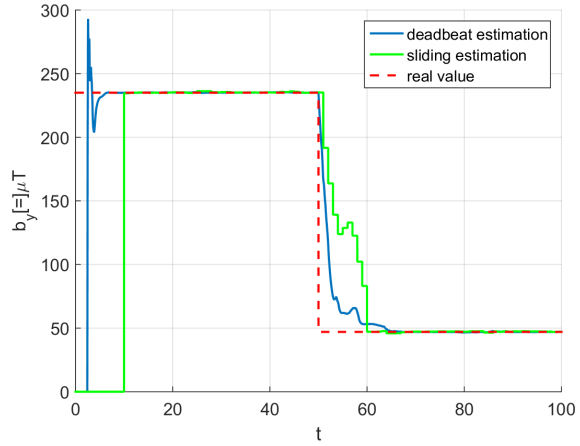

Fig. 5. Estimation results on y-axis in noisy scenario

he was writing a mail, then he put the phone in the pocket and finally the phone is hand-held while the user was walking (Fig. 8 shows the four described phases in terms of the gyroscope acquired measurements).

The sliding algorithm uses the same parameters chosen in the numerical test, the parameters for the deadbeat algorithm have been set to

$$\mu = 1, \quad \lambda = 0.1, \quad \rho = 1, \quad \varepsilon = 10^{-5}.$$

Figs 9, 10, 11 show the effectiveness of the estimation results in this real scenario.

Note that the proposed techniques provide an estimation $\hat{b}(t)$ comparable to the one obtained in the traditional way, i.e. $\tilde{b}$ but they do not require the sensor to be kept fixed in its center of gravity.

As highlighted by numerical and experimental results, although both the sliding and the deadbeat solutions exhibit good performance in estimating the hard iron bias, the latter technique shows better performance, in terms of convergence speed and robustness to noise, w.r.t. the first one.

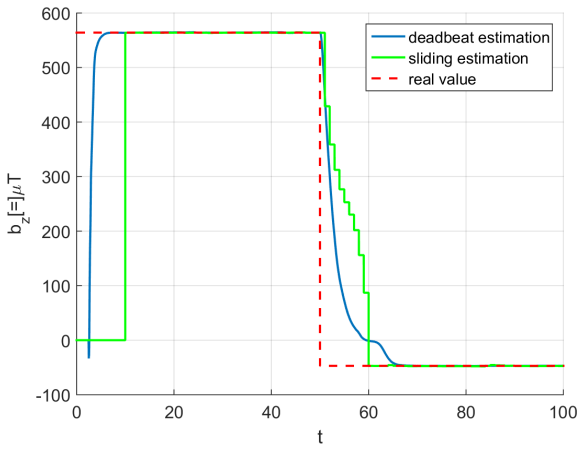

Fig. 6. Estimation results on z-axis in noisy scenario

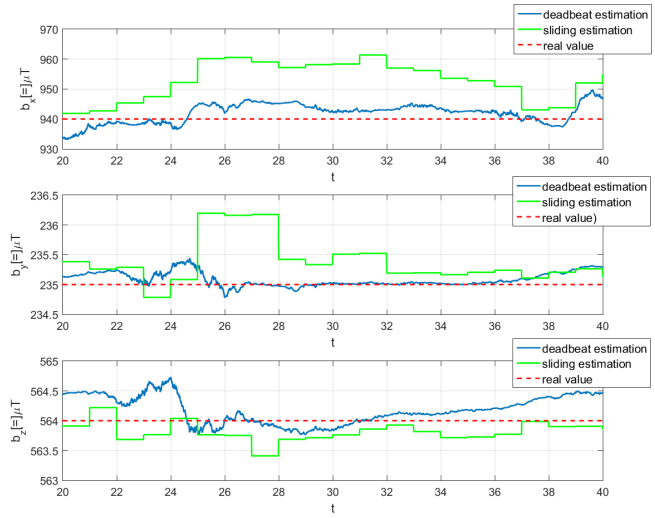

Fig. 7. zoom of estimation result in noisy scenario

VI. Conclusions

This paper faced the problem of estimating the hard iron bias affecting the measurements provided by a tri-axial magnetometer.

Two main algorithms, based on modulating functions and Volterra integral operator have been proposed, both of them ensuring finite-time estimation performance and robustness against measurements noise.

The effectiveness of the described solutions have been shown by numerical simulations and experimental tests carried out using a real magnetometer sensor equipped on a smartphone. Both numerical and experimental data have been acquired during standard use, with no requirements on the movements the sensor has to perform.

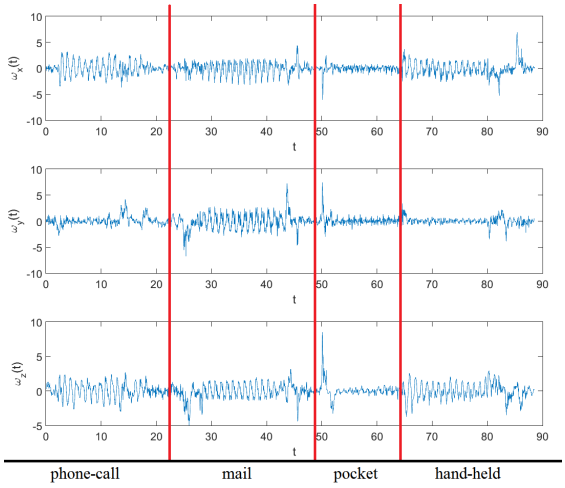

Fig. 8. Gyroscope measurements during the user walk - real experiment

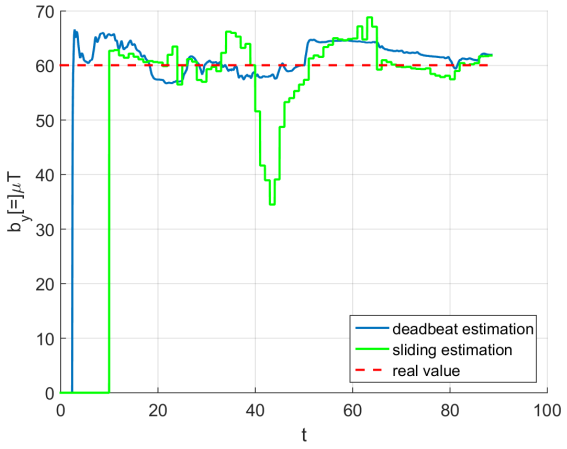

Fig. 10. Estimation results on y-axis in a real scenario

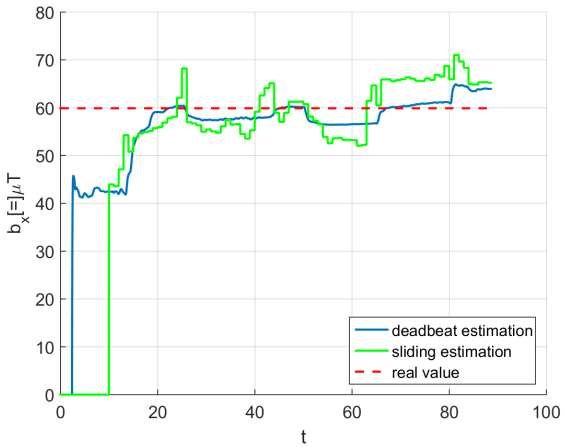

Fig. 9. Estimation results on x-axis in a real scenario

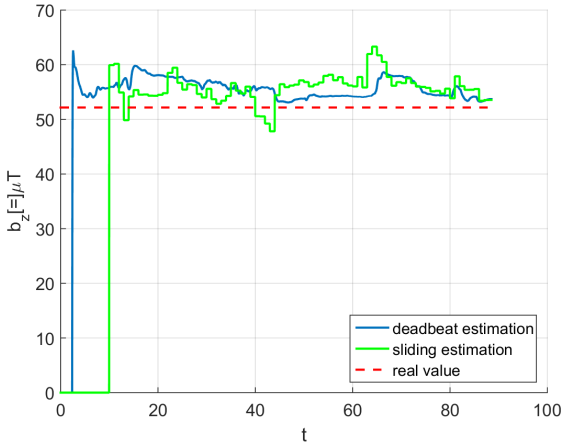

Fig. 11. Estimation results on z-axis in a real scenario

APPENDIX

THEORETICAL PRELIMINARIES

For the reader's convenience, some basic concepts of linear integral operators' algebra, of modulating functions (see [28], [34] and the references therein) and of rotations in the space, which are needed to derive the main results of the present work, will be briefly recalled.

A. $SO(3)$ properties

By definition, a rotation is a transformation that preserves the origin, Euclidean distance and orientation. Every rotation maps an orthonormal basis of $\mathbb{R}^3$ to another orthonormal basis. As a consequence, like any linear transformation of finite-dimensional vector spaces, a rotation can always be represented by a matrix. Moreover this rotation matrix is always an orthonormal matrix, i.e.

$$R^T R = R R^T = I \tag{A.36}$$

where I is the identity matrix of order 3.

Rotation matrices give a redundant description of frame orientation. They are characterized by nine elements which are not independent but related by a set of six constraints given by the orthonormality conditions. As a consequence, each matrix presents only three free parameters which are sufficient to describe orientation of a rigid body in $\mathbb{R}^3$. A representation of orientation in terms of three independent parameters constitutes a minimal representation and it can be obtained by using a set of three angles. Then, a generic rotation matrix can be obtained by composing a suitable sequence of three elementary rotations about single axes while guaranteeing that two successive rotations are not made about parallel axes. This implies that 12 distinct sets of angles are allowed out of all 27 possible combinations; each set represents a triplet of Euler angles. In the aeronautical field the most used triplet of Euler angles consists in the Roll-Pitch-Yaw (RPY) angles. Let R_2^1 be the rotation matrix from a first reference frame O_{1,x_1,y_1,z_1} to a second one O_{1,x_2,y_2,z_2}, the rotation resulting from RPY related to this matrix can be obtained as:

- a first rotation of an angle θ about the z_1-axis, the resulting rotated reference frame is O_{1,x_1',y_1',z_1}; this rotation is represented by an orthonormal matrix $R_{z_1}(\theta)$;
- a second rotation of an angle ψ about the y_1'-axis, the resulting rotated reference frame is $O_{1,x_1'',y_1',z_1'}$;

this rotation is represented by an orthonormal matrix $R_{y_1'}(\psi)$;

- a third rotation of an angle γ about the x_1''-axis, the resulting rotated reference frame is O_{1,x_2,y_2,z_2}; this rotation is represented by an orthonormal matrix $R_{x_1''}(\chi)$.

The complete rotation matrix can be finally obtained as

$$R_2^1 = R(\chi,\psi,\theta) = R_{x_1''}(\chi)R_{y_1'}(\psi)R_{z_1}(\theta) \tag{A.37}$$

Moreover, during a rotation variation, as shown in [35], by defining the skew-symmetric matrix

$$S(\omega(t)) = \begin{bmatrix} 0 & -\omega_z(t) & \omega_y(t) \\ \omega_z(t) & 0 & -\omega_x(t) \\ -\omega_y(t) & \omega_x(t) & 0 \end{bmatrix}, \tag{A.38}$$

the matrix $R(t) = R(\chi(t),\psi(t),\theta(t))$ satisfies the following property

$$\dot{R}(t) = R(t)S(\omega(t)) \tag{A.39}$$

B. Modulating functions

A function $\phi_K(t) \in C^K$ (K-times differentiable), defined over a finite-time interval $[0,T]$, which satisfies the following terminal conditions

$$\left.\frac{d^i\phi_K(t)}{dt^i}\right|_{t=0} = \left.\frac{d^i\phi_K(t)}{dt^i}\right|_{t=T} = 0, \forall i = 0,1,\ldots,K-1 \tag{A.40}$$

is called modulating function [28].

A function $f(t) \in \mathcal{L}^1$ over $[0,T]$ is modulated by taking the inner product with a modulating function $\phi_K(t)$

$$\langle f(t),\phi_K(t)\rangle = \int_0^T f(t)\phi_K(t)dt \tag{A.41}$$

The terminal constraints of (A.40) essentially make the boundary conditions of the function $f(t)$ irrelevant after modulations. Moreover, they make possible the transfer of the differentiation operation from the function $f(t)$ on to the modulating function $\phi_K(t)$, thereby eliminating the need to approximate time derivatives from noisy measurement data

$$\left\langle \frac{d^i f(t)}{dt^i},\phi_K(t)\right\rangle = (-1)^i \left\langle f(t), \frac{d^i\phi_K(t)}{dt^i}\right\rangle, i = 0,\ldots,K-1. \tag{A.42}$$

The class of spline-type modulating functions, namely ϕ_K^s, used in this paper is shown in Fig. 12. This class is characterized by two parameters: the order K of the highest derivative of ϕ_K^s, and the characteristic time $\overline{T}$; for a function ϕ_K^s, defined into the interval $[0,T]$, $\overline{T} = \frac{T}{K}$. The i-th derivative of a spline function, with order K and characteristic time $\overline{T}$, is expressed as

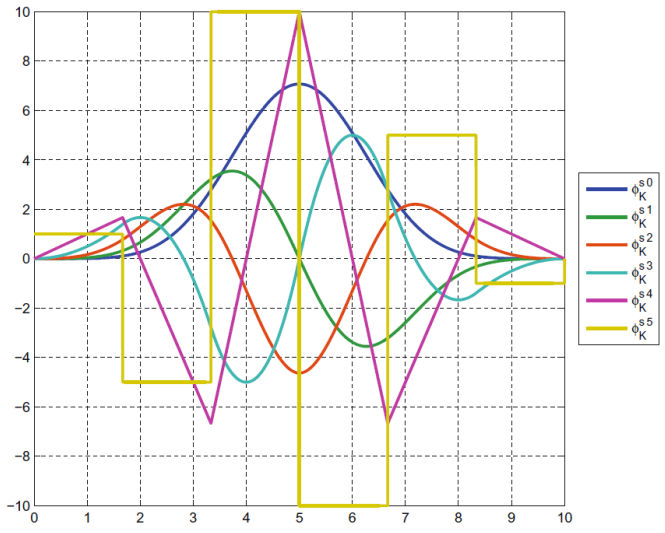

Fig. 12. Spline functions with $K = 6$ and $T = 10s$

$$\frac{d^i\phi_K^s(t)}{dt^i} = \begin{cases} \sum_{j=0}^{K}(-1)^j\binom{K}{j}g_{ji}(t-j\overline{T}), & i = 0,\ldots,K-1 \\ \sum_{j=0}^{K}(-1)^j\binom{K}{j}\delta(t-j\overline{T}), & i = K \end{cases} \tag{A.43}$$

where

$$g_{ij}(t-j\overline{T}) = \begin{cases} \frac{1}{(K-i-1)!}(t-j\overline{T})^{K-i-1}, & t \in [j\overline{T},T] \\ 0, & \text{otherwise,} \end{cases} \tag{A.44}$$

and $\delta(t)$ is the Dirac delta function.

C. Volterra integral operators algebra

Given a function $f \in \mathcal{L}^2_{loc}(\mathbb{R}_{\geq 0})$, its image through the Volterra (linear,integral) operator V_K induced by a Hilbert-Schmidt ($\mathcal{HS}$) Kernel Function $K(\cdot,\cdot) : \mathbb{R}\times\mathbb{R} \to \mathbb{R}$ is usually denoted by $[V_K f](\cdot)$, and is defined by the inner product:

$$[V_K f](t) \triangleq \int_0^t K(t,\tau)f(\tau)d\tau, t \in \mathbb{R}_{\geq 0} \tag{A.45}$$

Any explicit function of time $f(t) : t \leftarrow f_t \in \mathbb{R}$, such that $f(\cdot) \in \mathcal{L}^2_{loc}(\mathbb{R}_{\geq 0})$ will be addressed to as a signal. Then, given two scalars $a,b \in \mathbb{R}_{\geq 0}$, with $a < b$, let us denote by $f_{[a,b]}(\cdot)$ and $f_{(a,b]}(\cdot)$ the restriction of a signal $f(\cdot)$ to the closed interval $[a,b]$ and to the left open interval $(a,b]$, respectively. Moreover, let $f(t) \in \mathbb{R}^n, \forall t \geq 0$ be an i-times differentiable vector of signals, we denote by $f^{(i)}$ the vector of the i-th order time-derivative signals. Then, we recall the following useful definition:

Definition 1 *Weak (generalized) derivative Let $f(\cdot) \in \mathcal{L}^2_{loc}(\mathbb{R}_{\geq 0})$. $f^{(1)}(\cdot)$ is said a weak derivative of $f(\cdot)$ if*

$$\int_0^t f(\tau)\left(\frac{d}{d\tau}\gamma(\tau)\right)d\tau = -\int_0^t f^{(1)}(\tau)\gamma(\tau)d\tau, \forall t \in \mathbb{R}_{\geq 0}$$

for all $\gamma \in \mathcal{C}^\infty$, with $\gamma(0) = \gamma(t) = 0$.

We remark that $f^{(1)}(\cdot)$ is unique up to a set of zero Lebesgue measure, i.e., it is defined almost everywhere. If f is differentiable in the conventional sense, then its weak derivative is identical to its conventional derivative. Traditional rules for the derivation of sum or products of functions also hold for the weak derivative. Given a kernel function $K(\cdot,\cdot)$ in two variables, its i-th order weak derivative with respect to the second argument will be denoted as $K^{(i)}, i \in \mathbb{Z}_{\geq 0}$. For the sake of the implementability, a differential form to the operators will be devised by applying the Leibniz differentiation rule to the Volterra integral. The transformed signal $[V_K x](t), \forall t \geq 0$, can be obtained as the output of a system described by the scalar integro-differential equation:

$$\begin{cases} \dot{\xi}(t) = K(t,t)x(t) + \displaystyle\int_0^t \left(\frac{\partial}{\partial t}K(t,\tau)\right)x(\tau)d\tau, t \in \mathbb{R}_{\geq 0} \\ \xi(0) = \xi_0 = \int_0^t K(0,\tau)x(\tau)d\tau \end{cases}$$
$$[V_K x](t) = \xi(t), \forall t \in \mathbb{R}_{\geq 0}. \tag{A.46}$$

In the following some useful results dealing with the application of Volterra operators to the derivatives of a signal will be recalled.

Lemma 2 *Volterra image of a signal's derivative: For a given $i \geq 0$, consider a signal $f(\cdot) \in \mathcal{L}^2(\mathbb{R}_{\geq 0})$ that admits a i-th weak derivative in $\mathbb{R}_{\geq 0}$ and a kernel function $K(\cdot,\cdot) \in \mathcal{HS}$ that admits the i-th derivative (in the conventional sense) with respect to the second argument, $\forall t \in \mathbb{R}_{\geq 0}$. It holds that:*

$$\begin{aligned}[V_K f^{(i)}](t) = & \sum_{j=0}^{i-1}(-1)^{i-j-1}f^{(j)}(t)K^{(i-j-1)}(t) \\ & + \sum_{j=0}^{i-1}(-1)^{i-j}f^{(j)}(0)K^{(i-j-1)}(0) \\ & + (-1)^i[V_{K^{(i)}}f](t), \forall t \in \mathbb{R}_{\geq 0}\end{aligned} \tag{A.47}$$

that is, $[V_K f^{(i)}](\cdot)$ is non-anticipative with respect to $f(\cdot)$ and its first $(i-1)$-th derivatives $f^{(1)}(\cdot), \ldots, f^{(i-1)}(\cdot)$.

Lemma 2 allows to identify a class of kernels such that for each derivative $f^{(i)}, i \in \{0, \ldots, n-1\}$, the image signal $[V_K f^{(i)}](t), \forall t > 0$ is independent from the initial states $f(0), f^{(1)}(0), \ldots, f^{(i-1)}(0)$, according to the following definition.

Definition 2 *(i-th order non-asymptotic kernel):Consider a function $K(\cdot,\cdot)$ satisfying the assumptions of Lemma 2; if, in addition, for a given $i \geq 1$, the kernel verifies the condition*

$$K^{(j)}(t,0) = 0, \forall t \in \mathbb{R}_{\geq 0}, \forall j \in \{0, \ldots, i-1\}, \tag{A.48}$$

then, it is called an i-th order non-asymptotic kernel.

Assuming that $K(\cdot,\cdot)$ is an n-th order non-asymptotic kernel function, then it holds that:

$$\begin{aligned}[V_K f^{(i)}](t) = & \sum_{j=0}^{i-1}(-1)^{i-1-j}f^{(j)}(t)K^{(i-j-1)}(t,t) \\ & + (-1)^i[V_{K^{(i)}}f](t), i \in \{1, \ldots, n-1\}.\end{aligned} \tag{A.49}$$

Considering the case $i = 1$, by some trivial manipulation of (A.49) it follows that

$$[V_K f^{(1)}](t) = f(t)K(t,t) - [V_{K^{(1)}}f](t). \tag{A.50}$$

Moreover, changing the kernel K with $K^{(j)}$, for any $j \in \{1, \ldots, n-1\}$, the following integral equation holds, too:

$$[V_{K^{(j)}}f^{(i+1)}](t) = f^{(i)}(t)K^{(j)}(t,t) - [V_{K^{(j+1)}}f^{(i)}](t). \tag{A.51}$$

Let now $K(t,\tau)$ be the following Bivariate Feedthrough Non-asymptotic Kernels (BF-NK)

$$K(t,\tau) = e^{-\rho_h(t-\tau)}(1 - e^{\overline{\rho}\tau})^N,$$

where $\overline{\rho}, \rho_h \in \mathbb{R}_{\geq 0}$ are arbitrarily set constant parameters.

Note for any $i \in \{0, 1, \ldots, N\}$, the i-th order weak derivative w.r.t. the second argument, τ, is

$$K^{(i)}(t,\tau) = e^{-\rho_h t}\frac{d^i}{d\tau^i}[(1 - e^{\overline{\rho}\tau})^N] \tag{A.52}$$

with $K^{(i)}(t,\tau) = 0, \forall t \in \mathbb{R}_{\geq 0}, i \in \{0, 1, \ldots, N\}$.

For the chosen kernel function, for any $i \in \{1, \ldots, N\}$, the partial derivative w.r.t. the first argument t satisfies

$$\frac{\partial}{\partial t}K^{(i)}(t,\tau) = -\rho_h K^{(i)}(t,\tau). \tag{A.53}$$

As a consequence, the first equation in the state space (A.46) is:

$$\begin{aligned}\dot{\xi} &= K^{(i)}(t,t)f(t) + \textstyle\int_0^t (\frac{\partial}{\partial t}K^{(i)}(t,\tau))f(\tau)d\tau \\ &= K^{(i)}(t,t)f(t) - \rho_h\xi(t), \forall t \in \mathbb{R}_{\geq 0} \\ \xi(0) &= \xi_0 = 0.\end{aligned} \tag{A.54}$$

Being $K^{(i)}(t,t)$ bounded, it holds that the scalar dynamical system realization of the Volterra operators induced by the proposed kernels is internally stable. At this point, the basic principle of non-asymptotic kernel-based estimation and the way to calculate auxiliary signals through the Volterra operator have been recalled. In the next Section the deadbeat estimation algorithm for the ferromagnetic bias affecting magnetometers measurements will be presented.

CONVERGENCE TIME COMPUTATION

Lemma 3 *Deadbeat estimation algorithm convergence time: Let $V(t) > 0, \forall t \geq t_0$, and let*

$$\dot{V}(t) \leq -cV^\eta(t), \forall t \geq t_0,$$

with $c > 0$ and $\eta \in (0,1)$, be the function time derivative; then

$$\begin{cases} V^{1-\eta}(t) \leq V^{1-\eta}(t_0) - c(1-\eta)(t-t_0), & t \in [t_0, t_1] \\ V(t) = 0, & \forall t \geq t_1, \end{cases}$$

with

$$t_1 = t_0 + \frac{V^{1-\eta}(t_0)}{c(1-\eta)}.$$

Proof: Let the following differential equation holds

$$\begin{cases} \dot{x}(t) = -cx^{\eta}(t) \\ \\ x(t_0) = V(t_0). \end{cases}$$

The solution of the above equation is

$$x^{1-\eta}(t) = -c(1-\eta)(t-t_0) + x^{1-\eta}(t_0),$$

the derivative of which is

$$\frac{d}{dt}x^{1-\eta}(t) = -c(1-\eta) < 0,$$

then the function $x^{1-\eta}(t)$ is monotonically decreasing; as a consequence

$$V^{1-\eta}(t) \leq V^{1-\eta}(t_0) - c(1-\eta)(t-t_0), \forall t_0 \leq t \leq t_1.$$

Moreover $V^{1-\eta}(t_1) = 0$ where

$$t_1 = t_0 + \frac{V^{1-\eta}(t_0)}{c(1-\eta)}.$$

Since $V^{1-\eta}(t)$ is monotonically decreasing and $V(t) \geq 0$ then $V(t)$ is monotonically decreasing too and

$$V(t) = 0, \forall t \geq t_1.$$

■

REFERENCES

[1] A. A. Kaufman, R. L. K. Kleinberg, and R. O. Hansen, *Principles of the Magnetic Methods in Geophysics*, vol. 12 of Methods in Geochemistry and Geophysics, Elsevier Science, New York, NY, USA, 2008.

[2] R.G. Valenti, I. Dryanovski, J. Xiao, *A Linear Kalman Filter for MARG Orientation Estimation Using the Algebraic Quaternion Algorithm*, IEEE Transactions on Instrumentation and Measurement, vol.65, no.2, pp.467-481, Feb. 2016.

[3] F.L. Markley, *Attitude determination and parameter estimation using vector observations: Theory*, The Journal of the Astronautical Sciences, 37(1):4158, 1989.

[4] A.-J. Baerveldt and R. Klang, *A low-cost and low-weight attitude estimation system for an autonomous helicopter*, Intelligent Engineering Systems, 1997.

[5] J. L. Marins, X. Yun, E. R. Backmann, R. B. McGhee, and M. Zyda, *An extended kalman filter for quaternion-based orientation estimation using marg sensors*, in IEEE/RSJ International Conference on Intelligent Robots and Systems, 2001, pp. 20032011.

[6] D. Gebre-Egziabher, R. Hayward, and J. Powell, *Design of multi-sensor attitude determination systems*, IEEE Transactions on Aerospace and Electronic Systems, vol. 40, no. 2, pp. 627649, April 2004.

[7] J. L. Crassidis, F. L. Markley, and Y. Cheng, *Nonlinear attitude filtering methods*, Journal of Guidance, Control,and Dynamics, vol. 30, no. 1, pp. 1228, January 2007.

[8] J. Vcelak, P. Ripka, A. Platil, J. Kubik and P. Kaspar, *Errors of AMR compass and methods of their compensation*, Sensors Actuators 129, 53-7, 2006.

[9] D. Gebre-Egziabher, G.H. Elkaim, J.D. Powell and B.W. Parkinson, *Calibration of strap-down magnetometers in magnetic field domain*, J. Aerosp. Eng. 19, 2006.

[10] T. Liu, Y. Inoue and K. Shibata, *A simplified magnetometer calibration method to improve the accuracy of three-dimensional orientation measurement*, ICIC Express Lett. 6, 2012.

[11] W.T. Fong, S.K. Ong and A.Y.C. Nee, *Methods for in-field user calibration of an inertial measurement unit without external equipment*, Meas. Sci. Technol. 19, 2008.

[12] T. Pylvanainen, *Automatic and adaptive calibration of 3D field sensors*, Appl. Math. modelling 32, 2008.

[13] D. Gebre-Egziabher, *Magnetometer autocalibration leveraging measurement locus constraints*, J. Aircr. 44, 2007.

[14] F. Primdahl, *Instrumentos Geomagneticos*, Publicações do Observatório Nacional do Brasil 09, 1986

[15] J.F. Vasconcelos, G. Elkaim, C. Silvestre, P. Oliveira and B. Cardeira, *Geometric approach to strap-down magnetometer calibration in sensor frame*, IEEE Trans. Aerosp. Electron. Syst. 47, 2011.

[16] J.C. Fang, H.W. Sun, J.J. Cao, X. Zhang and Y. Tao, *A novel calibration method of magnetic compass based on ellipsoid fitting*, IEEE Trans. Instrum. Meas. 60, 2011.

[17] S. Bonnet, C. Bassompierre, C. Godin, S. Lesecq and A. Barraud, *Calibration methods for inertial and magnetic sensors*, Sensors Actuators 156, 2009.

[18] V. Renaudin, M.H. Afzal and G. Lachapelle, *New method for magnetometers based orientation estimation*, Rec. IEEE PLANS Position Locat. Navig. Symp., Indian Wells, CA, USA, pp. 335-340, 2010.

[19] I. Markovsky, A. Kukush, and S. Van Huffel. *Consistent least squares fitting of ellipsoids*, Numerische Mathematik, 98(1):177194, 2004

[20] V. Renaudin, M.H. Afzal, and G. Lachapelle, *Complete triaxis magnetometer calibration in the magnetic domain*, Journal of Sensors, 2010.

[21] T. Neubert,*CSC-OVH in-flight calibration Ørsted technical note*, TN-264, 1995

[22] J.F. Vasconcelos, G. Elkaim, C. Silvestre, P. Oliveira and B. Cardeira, *A Geometric Approach to Strapdown Magnetometer Calibration in Sensor Frame*, IEEE Transactions on Aerospace and Electronic Systems, Volume:47, 2001.

[23] M. Kok and T.B. Scön,*Maximum likelihood calibration of a magnetometer using inertial sensors*, Proceedings of the 19th World Congress of the International Federation of Automatic Control (IFAC), pp. 92-97, Cape Town, South Africa, August 2014.

[24] R. Alonso and M.D. Shuster, *Complete linear attitude-independent magnetometer calibration*, The Journal of the Astronautical Sciences, 50(4):477490, 2002.

[25] B. Gambhir, *Determination of Magnetometer Biases Using Module RESIDG*, Technical Report 3000-32700-01TN, Computer Sciences Corporation, March 1975.

[26] http://www.ecnmag.com/article/2014/12/magnetometer-2d-calibration-accurate-angle-computation

[27] http://www.vectornav.com/support/library/magnetometer

[28] G. Fedele, L. Coluccio, *A recursive scheme for frequency estimation using the modulating functions method*, Applied Mathematics and Computation, Volume 216, Issue 5, 1 May 2010, Pages 1393-1400.

[29] D. Liu, T. Laleg-Kirati, O. Gibaru, W. Perruquetti, *Identification of fractional order systems using modulating functions method*, 2013 American Control Confer- ence, 2013, Jun 2013, Washington, DC, United States, 2013.

[30] G. Pin, A. Assalone, M. Lovera, and T. Parisini, *Kernel-based Non-Asymptotic Parameter Estimation of Continuous-time Systems*, 51st IEEE Conference on Decision and Control December 10-13, 2012. Maui, Hawaii, USA.

[31] G. Pin, C. Boli, T. Parisini, *Deadbeat kernel-based frequency estimation of a biased sinusoidal signal*, European Control Conference (ECC), 2015, pp.479-484, 15-17 July 2015.

[32] www.mathworks.com

[33] R. Mahony, T. Hamel, and J. Pflimlin, *Non-linear complementary filters on the special orthogonal group*, IEEE Transactions on Automatic Control, vol.53, no.5, pp.1203-1218, June 2008.

[34] T. Burton, *Volterra Integral and Differential Equations*, Elsevier, 2005.

[35] B. Siciliano, L. Sciavicco, L. Villani, G. Oriolo, *Robotics: Modelling, Planning and Control*, Springer Publishing Company, Incorporated, 2008.